IEEE Photonics Journal
An IEEE Photonics Society Publication

Open Access

Interleaved Subwavelength Gratings Strip Waveguide Based TM Pass Polarizer on SOI Platform

Volume 12, Number 2, April 2020

Zhengying Xu
Tao Lyu
Xiaohan Sun

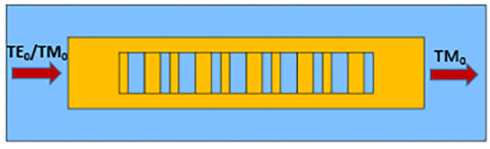

Interleaved subwavelength gratings strip waveguide based TM-pass polarizer

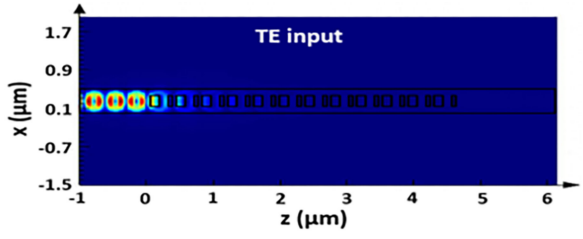

Light distribution of TE mode

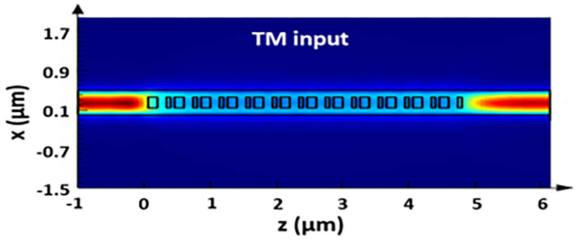

Light distribution of TM mode

DOI: 10.1109/JPHOT.2020.2968570

Interleaved Subwavelength Gratings Strip Waveguide Based TM Pass Polarizer on SOI Platform

Zhengying Xu, Tao Lyu, and Xiaohan Sun

National Research Center for Optical Sensing/Communications Integrated Networking, Southeast University, Nanjing 210096, China

DOI:10.1109/JPHOT.2020.2968570

Manuscript received January 16, 2020; accepted January 19, 2020. Date of publication January 21, 2020; date of current version March 9, 2020. Corresponding author: Xiaohan Sun (e-mail: xhsun@seu.edu.cn).
This article has supplementary downloadable material available at https://ieeexplore.ieee.org, provided by the authors.

Abstract: We report on an ultra-compact, low loss and broadband TM-pass polarizer, which is constructed by two interleaved subwavelength-gratings (SWGs) waveguides inserted in the center of the strip waveguide on a silicon-on-insulator (SOI) platform. The device structure is optimally engineered to support Bloch mode for fundamental TM polarization only. Therefore, the TM mode transmits along the strip waveguide with rather low propagation loss while the TE mode is completely reflected by the embedded SWGs waveguides. Simulation results show that an efficient and ultra-compact TM-pass polarizer of 5.2 μm in length is realized with extinction ratio (ER) of 31.63 dB and insertion loss (IL) of 0.18 dB at the operating wavelength of 1550 nm. The operation bandwidth for ER over 20 dB and IL below 0.32 dB is 155 nm (from 1465 to 1620 nm). By increasing the period number, the ER performance and bandwidth can be further improved. Furthermore, the fabrication of the present polarizer only requires mono-lithography and single etch process, which will greatly reduce the fabrication difficulty.

Index Terms: Subwavelength gratings (SWGs), polarization controlling, polarizer, integrated optical devices.

1. Introduction

Silicon-on-Insulator (SOI) has been regarded as a promising platform for silicon photonics since it has great features of well-established CMOS processing and high refractive index contrast [1]. However, photonic devices based on SOI nanowires usually suffer from strong polarization dependent issues, which will limit their applications in photonic integrated circuits (PICs). Hence, polarization manipulate is a crucial part of PICs [2]. As one of the typical polarization-manipulating devices, polarizers have been well developed in recent years to realize a polarization transparent circuit. In previous studies, various high-performance polarizers have been demonstrated for the applications of PICs [3]–[7]. Considering the TE mode is prevailing used in the practical applications, these polarizers are designed to extinguish the unwanted TM polarization state and reserve the desired TE polarization state to realize TE mode waveguides. Compared with the TE mode waveguide, the TM mode waveguide can provide a more promising way for the highly sensitive sensing applications since TM polarization has stronger interactions of evanescent wave than that of TE polarization [8]. In the past years several configurations of TM-pass polarizers have been reported

[9]–[15]. By utilizing 300 nm thick silicon core layer, Wang *et al.* [10] proposed a CMOS compatible TM-pass polarizer of 10 μm in length with a negligible insertion loss (IL) and high extinction ratio (ER) performance. In [13], a novel TM-pass polarizer using HPGs structure is realized with an ultra-compact size of 2.6 μm long. However, the bandwidth is not wide enough and the fabrication process of such structure is complicated. In Ref [14], a 150 μm long graphene-based TM-pass polarizer with ER greater than 40 dB over 100 nm operation bandwidth has been proposed. In [15], another improved TM-pass polarizer using highly doped p-silicon has been reported with ER of 30 dB and length of 15 μm. However, these devices are suffering from high propagation loss. Since a device performance is reflected by its synthesized indicators, it is necessary to develop a novel TM-pass polarizer which can meet the requirements of ultra-compact size, ultra-broad bandwidth, high extinction ratio, low propagation loss and easy fabrication process simultaneously.

Subwavelength gratings (SWGs), basically consisting of periodic cross-distributed high and low refractive index materials, offer a promising way to implement novel photonic devices [16], [17]. Since the operating wavelength is larger than the grating period, light propagating in SWG waveguide can be treated as it passes through a strip waveguide with equivalent homogeneous material core [18]. By adjusting the duty cycles of the high and low refractive index materials in one SWG period, the optical properties of the SWG waveguide can be tailored and modified for a given application [19]. Owing to these unique properties, various kinds of photonic devices based on SWGs structures have been proposed, for instance, directional couplers [20], [21], contra-directional couplers [22], polarization-insensitive grating couplers [23], polarization beam splitters [24], [25], rotators [26], [27], polarizers [28], [29], filters [30], [31], and resonators [32]. In [29], Guan and Dai propose a TM-pass polarizer with 9 μm in length by treating the SWG waveguide as a Bragg reflector. However, this device suffers from a narrow bandwidth (the bandwidth for ER over 20 dB is 60 nm). In [30], a SWG-Based TM-pass filter is demonstrated. By engineering the SWGs waveguide parameters, the proposed polarizer with 4.2 μm long is achieved. However, the lowest IL of the present device in the whole calculation region is 1 dB, such high propagation loss will be detrimental to the realization of high-performance system. Hence, a compact polarizer with high ER, low IL and broad bandwidth is highly desired to improve the PICs performance.

In this paper, we present an ultra-compact, low-loss and broadband TM-pass polarizer by utilizing two interleaved SWGs waveguides inserted in the center of silicon-based strip waveguide on SOI platform. In our design, the structure parameters are carefully engineered to make sure only Bloch mode of fundamental TM polarization is supported in the present device. For TE polarization, this device acts as a Bragg reflector. Therefore, the inject TM polarization will transmit along the SWG-based silicon waveguide with rather low propagation loss while the TE polarization will reflect by the interleaved SWGs waveguides during the propagation. The calculation results show that the designed polarizer is about 5.2 μm long, the ER and IL are 31.63 dB and 0.18 dB, respectively, at the operation wavelength of 1550 nm. The bandwidth for ER $>$ 20 dB and IL $<$ 0.32 dB is 155 nm (from 1465 to 1620 nm). Additionally, the present device fabrication only requires a single-etch process, which will make the fabrication process much simpler.

2. Design Structure and Principle

The proposed TM-pass polarizer is designed using a 220 nm thick silicon layer on an SOI platform, as shown in Fig. 1. The basic structure of the polarizer is made of a silicon strip waveguide with silica upper cladding. Two interleaved SWGs waveguides with the same waveguide widths are inserted into the center of the strip waveguide, form the polarizer section. For these two SWGs waveguides, the period and duty cycle are denoted as $\boldsymbol{\Lambda_1}(\boldsymbol{\Lambda_2})$ and $\boldsymbol{\eta_1}$ ($\boldsymbol{\eta_2}$), respectively. The widths of strip waveguide and SWGs waveguides are w_1 and $\boldsymbol{w_2}$, The active length of the device is L. Here one has $\boldsymbol{L = N\Lambda}$, where the period Λ is denoted as $\boldsymbol{\Lambda = \Lambda_1 + \Lambda_2}$ and N is the period number.

As mentioned before, a simplified approximation method for SWGs structure is that a SWGs can be treated as a homogenous material (*HM)* [17]. After this approximation, a SWG-based waveguide can be considered as a traditional waveguide using HM with refractive index of $\boldsymbol{n_{eq}}$. The most commonly used approximation methods for calculating the equivalent refractive index of

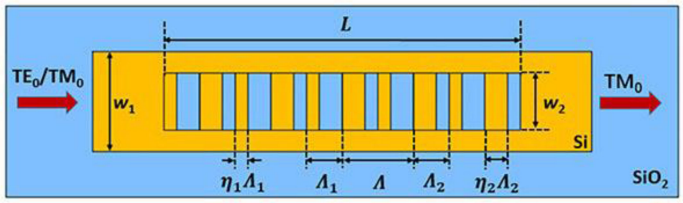

Fig. 1. Schematic configuration of the proposed TM pass polarizer on SOI platform with silica cladding.

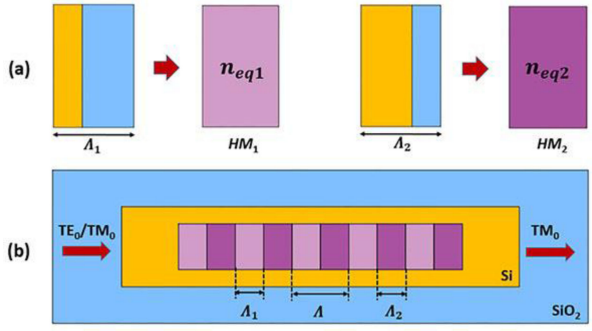

Fig. 2. Schematic of equivalent polarizer. (a) the SWG represented as homogenous material with equivalent refractive index n_{eq}. (b) Top view of the proposed polarizer with SWG region replaced by the homogenous medium waveguides.

SWGs structure are the effective medium theory [33] and coupled mode theory [34]. Considering the equivalent refractive indices calculation based on high order approximation of the effective medium theory has heavy computing burden and also very time consuming; here we use the fast and predigest coupled mode theory approach to determine the device parameters roughly. The refractive index step of the *HM*, $\boldsymbol{\Delta n_{eq}}$, is given by [34]:

$$\boldsymbol{\Delta n_{eq}} = \eta \boldsymbol{\Delta n} \tag{1}$$

where η is the duty cycle and $\boldsymbol{\Delta n}$ is the refractive index step between alternated low and high index materials of the SWG waveguide. Based on this method, the two interleaved SWGs waveguides in our design can be replaced by two cross-distributed equivalent *HM* waveguides. We label SWGs waveguide with period $\boldsymbol{\Lambda}_1$ ($\boldsymbol{\Lambda}_2$) as $\boldsymbol{HM}_1$ ($\boldsymbol{HM}_2$). The equivalent refractive index of $\boldsymbol{HM}_1$ and $\boldsymbol{HM}_2$ are $\boldsymbol{n_{eq1}}$ and $\boldsymbol{n_{eq2}}$, respectively, as shown in Fig. 2(a). After this equivalent, the original SWGs region can be regard as a new HM-based structure with period $\boldsymbol{\Lambda}$ and duty cycle $\boldsymbol{\Lambda}_1/\boldsymbol{\Lambda}$, as shown in Fig. 2(b). To obtain a TM-pass polarizer, the structural parameters should be modified carefully to satisfy the following Bragg grating equations [35]

$$\boldsymbol{n_{eff1}^{TE}}\boldsymbol{\Lambda}_1 + \boldsymbol{n_{eff2}^{TE}}\boldsymbol{\Lambda}_2 = \lambda_0/2 \tag{2}$$

$$\boldsymbol{n_{eff1}^{TM}}\boldsymbol{\Lambda}_1 + \boldsymbol{n_{eff2}^{TM}}\boldsymbol{\Lambda}_2 < \lambda_0/2 \tag{3}$$

where λ_0 is the operating wavelength, $\boldsymbol{n_{eff1}^{TE}}$ ($\boldsymbol{n_{\text{eff1}}^{TM}}$) and $\boldsymbol{n_{eff2}^{TE}}$ ($\boldsymbol{n_{eff2}^{TM}}$) are the effective indices of the fundamental TE (TM) mode in the $\boldsymbol{HM}_1$ and $\boldsymbol{HM}_2$ sections. $\boldsymbol{\Lambda}_1$ and $\boldsymbol{\Lambda}_2$ are the length of $\boldsymbol{HM}_1$ and $\boldsymbol{HM}_2$ section region. Under this condition, only the Bloch mode for TM polarization is supported in the present device. When the TM polarization enters the device, it directly passes through the silicon waveguide with a very little propagation loss. When the TE polarization enters, it will be significantly reflected due to the high efficiency Bragg reflection caused by the embedded structure.

As an example, the widths of the strip and SWGs waveguides are chosen as $\boldsymbol{w}_1 = 500$ nm and $\boldsymbol{w}_2 = 200$ nm, respectively. Since these are two different SWGs waveguides, for simplicity, we assume $\boldsymbol{\Lambda}_1 = \boldsymbol{\Lambda}_2$ in our design. If not specified, the operating wavelength is kept constant as

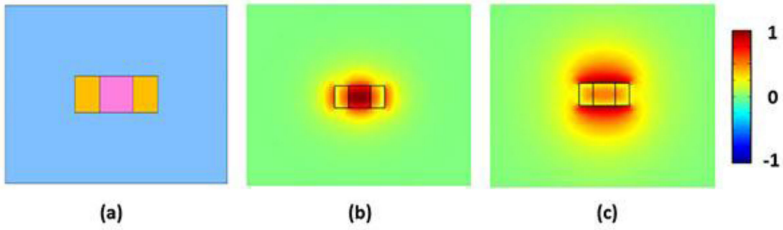

Fig. 3. (a) cross section view of the polarizer section with a homogenous medium core. Field distributions of (b) TE mode and (c) TM mode in the polarizer section. The dimensions are $w_1 = 500$ nm, $w_2 = 200$ nm and $\eta = 0.4$.

1550 nm. The period number N is taken as 13, by default. The reflective indices of silicon and silica are $\boldsymbol{n_{Si}} = 3.478$ and $\boldsymbol{n_{SiO2}} = 1.445$ in the following calculation.

3. Results and Discussions

To better understand the operating principle of the designed polarizer, a finite element method is utilized to analyze the mode characteristics of polarizer section. The field profiles for fundamental TE and TM modes of the polarizer section at the operating wavelength are illustrated in Fig. 3. According to the equivalent refractive index method of SWGs structure [28], the $\boldsymbol{n_{eq}}$ of $\boldsymbol{HM}$ is lower than the refractive index of silicon. Therefore, the polarizer section can be regard as a vertical slot waveguide, as shown in Fig. 3(a). From Fig. 3(b) one can see that the fundamental TE mode is highly confined in the "slot" region, which is benefit for the interaction between light field and SWGs Bragg gratings. For the fundamental TM mode, the filed distribution in the polarizer section is similar to that in a vertical slot waveguide, as shown in Fig. 3(c). It is noticeable, however, the "slot" width in our design is wider than that of traditional slot waveguide, leading to an increased evanescent field leaked into the surrounding materials.

In order to realize an efficient polarizer, periods and duty cycles of the two interleaved SWGs waveguides should be properly selected to make sure that the fundamental TE mode is totally reflected at the operating wavelength while there is no affected to TM mode. A 3D finite-difference time-domain (3D-FDTD) method is employed to evaluate the ER and IL performances for TE mode at the operation wavelength. The ER and IL are defined as below:

$$\mathbf{ER(dB)} = \mathbf{10}\log_{10}\frac{\boldsymbol{P^O_{TE}}}{\boldsymbol{P^O_{TM}}} \tag{4}$$

$$\mathbf{IL(dB)} = \mathbf{10}\log_{10}\frac{\boldsymbol{P^O_{TE}}}{\boldsymbol{P^I_{TE}}} \tag{5}$$

where $\boldsymbol{P^I_{TE}}$ stands for the input port power of TE polarization, $\boldsymbol{P^O_{TE}}$ and $\boldsymbol{P^O_{TM}}$ stand for the output port power of TE and TM polarizations, respectively. The grid resolution used in the simulation is $\boldsymbol{\Delta x \times \Delta y \times \Delta z = 20 \times 20 \times 20\ nm^3}$. Optical properties and the ER (IL) performance of the present polarizer as functions of η_1 and η_2 are summarized in Table 1. Both η_1 and η_2 are kept between 0.3 and 0.7 to make sure that the SWG fin width is within the limitation range of the fabrication requirement, since the minimum feature size has been realized in fabrication is 50 nm [9], [36]. In addition, the reflection peak (Bragg wavelength) of TE mode is kept at 1550 nm. According to the approximation method, the gratings period has been roughly determined, as shown in the seventh column of the Table 1. Considering this approximation method does not take the scattering loss caused by the refractive index modulation into account, the device transmission features are calculated with the actual SWGs structure and the roughly determined period to reduce the effect of approximation error on device performance estimation. From Table 1 one can see that when η_1 is fixed, the one with period "Λ" shows a descend trend as η_2 is increased. It is noted that the ER

TABLE 1
SWG Geometries, Optical Properties and Device Performances at 1550 nm

η_1	η_2	Δn_{eq1}	Δn_{eq2}	n_{eff1}^{TE}	n_{eff2}^{TE}	Λ (nm)	ER (dB)	IL (dB)
0.3	0.4	0.6099	0.8132	1.6857	1.7816	447	3.97	0.35
0.3	0.5	0.6099	1.0165	1.6857	1.8847	434	12.37	0.27
0.3	0.6	0.6099	1.2198	1.6857	1.9923	421	21.17	0.20
0.3	0.7	0.6099	1.4231	1.6857	2.103	409	27.87	0.13
0.4	0.3	0.8132	0.6099	1.7816	1.6857	447	1.88	0.36
0.4	0.5	0.8132	1.0165	1.7816	1.8847	423	2.76	0.21
0.4	0.6	0.8132	1.2198	1.7816	1.9923	411	9.83	0.14
0.4	0.7	0.8132	1.4231	1.7816	2.103	399	18.09	0.08
0.5	0.3	1.0165	0.6099	1.8847	1.6857	434	6.65	0.28
0.5	0.4	1.0165	0.8132	1.8847	1.7816	423	1.85	0.22
0.5	0.6	1.0165	1.2198	1.8847	1.9923	400	2.93	0.07
0.5	0.7	1.0165	1.4231	1.8847	2.103	389	8.83	0.04
0.6	0.3	1.2198	0.6099	1.9923	1.6857	421	17.43	0.22
0.6	0.4	1.2198	0.8132	1.9923	1.7816	411	5.49	0.16
0.6	0.5	1.2198	1.0165	1.9923	1.8847	400	1.78	0.08
0.6	0.7	1.2198	1.4231	1.9923	2.103	378	3.93	0.01
0.7	0.3	1.4231	0.6099	2.103	1.6857	409	26.04	0.17
0.7	0.4	1.4231	0.8132	2.103	1.7816	399	15.41	0.10
0.7	0.5	1.4231	1.0165	2.103	1.8847	389	7.42	0.07
0.7	0.6	1.4231	1.2198	2.103	1.9923	378	2.42	0.01

performance is significantly improved with the increasing of duty cycle step $\Delta\eta$ ($\Delta\eta = |\eta_1 - \eta_2|$). This is because the decreasing of $\Delta\eta$ will lead the equivalent refractive index of $\boldsymbol{HM}_1$ close to that of $\boldsymbol{HM}_2$, thereby reducing the Bragg reflecting efficiency of the TE mode. On the other hand, the IL performance is gradually ameliorated with the increasing of the duty cycle η since the higher η will reduce the radiation loss of TM mode, as mentioned in previously report [13]. Since there is no single optimum parameter that can maintain maximized ER and minimum IL simultaneously, we choose $\eta_1 = \mathbf{0.3}$ and $\eta_2 = \mathbf{0.7}$ as a trade-off. Under this condition, the calculated period Λ is 409 nm, the corresponding IL and ER are 0.13 dB and 27.87 dB, respectively, at the operating wavelength.

The optimal value of the period Λ is determined by calculating the transmission responses of Eigen modes. The transmission and reflection responses of the present device as a function of period Λ for both polarizations are shown in Fig. 4. It is obviously that for the inject TE mode the period Λ has a notable influence on the transmission/reflection behavior since the operation mechanism of the device is highly sensitive to the Λ variation, as shown in Fig. 4(a). For the inject TE mode, the transmission reaches its minimum value of -29.78 dB and the corresponding reflection value is -0.244 dB when the period Λ is 400 nm. On the other hand, the lowest reflection in the calculation region is -0.226 dB and the corresponding transmission is -28.79 dB ($\Lambda =$ 391 nm) for the TE mode. From Fig. 4(b) one can see that the performance of the inject TM mode is slightly affected by the Λ variation, since the Bloch wave of TM polarization is supported in the

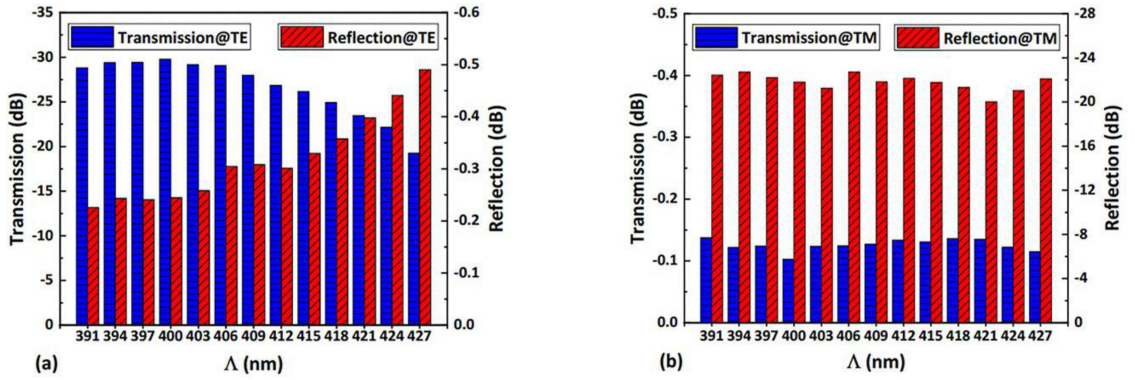

Fig. 4. Transmission and reflection responses of the proposed device as a function of period Λ. (a) TE mode and (b) TM mode input. The other dimensions are $w_1 = 500$ nm, $w_2 = 200$ nm, $\eta_1 = 0.3$ and $\eta_2 = 0.7$.

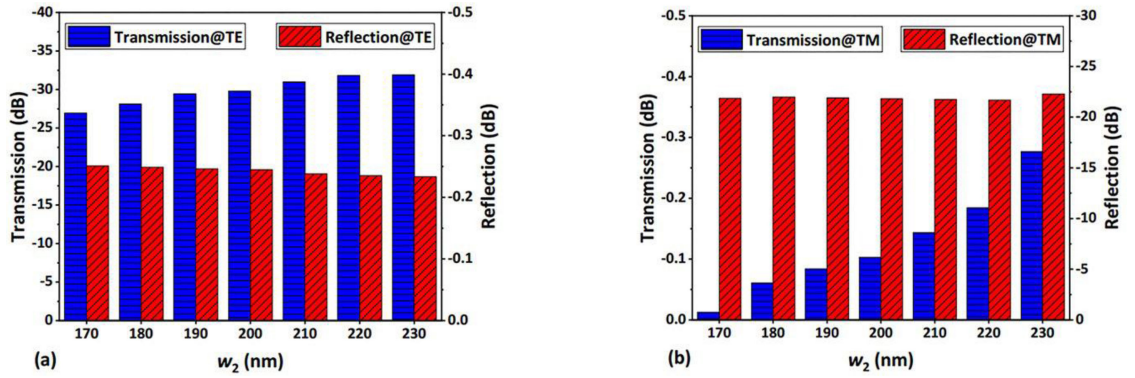

Fig. 5. Transmission and reflection responses of the device as a function of SWG waveguides width w_2. (a) TE mode input. (b) TM mode input. The other dimensions are $w_1 = 500$ nm, $\Lambda = 400$ nm, $\eta_1 = 0.3$ and $\eta_2 = 0.7$.

present device. For the TM mode, the minimum value of transmission (reflection) is -0.103 dB (-22.71 dB) and the corresponding reflection (transmission) value is -21.79 dB (-0.122 dB), respectively, at the period of 400 nm (394 nm). Take full account of the transmission and reflection value at different period condition, one can see that the optimum period value is $\Lambda = 400$ nm. The corresponding transmission and reflection responses for TE (TM) polarization are -29.78 dB (-0.103 dB) and -0.244 dB (-21.79 dB), respectively.

To further improve the device performance, the influence of the SWGs waveguides width is also studied. Fig. 5 illustrates the calculated responses of transmission/reflection for both polarizations as the SWGs waveguides width w_2 varies. From Fig. 5(a) one can see that the transmission response of TE polarization is gradually decreased from -26.93 dB to -31.89 dB and the reflection response is slightly increased from -0.251 dB to -0.233 dB when w_2 ranges from 170 nm to 230 nm, indicates an enhanced Bragg reflection efficiency. This is because by increasing w_2, more electric field of TE mode will be confined in the embedded SWG waveguides, leading to a stronger light-matter interaction. For inject TM mode, the reflection response is not sensitive to the w_2 since the embedded silicon waveguide works as a traditional slot waveguide for the TM polarization. However, the transmission response gradually deteriorates with the increasing of w_2, since the increased slot width will introduce higher radiation loss for TM mode. In addition, the transmission response decreases more rapidly when the w_2 is over 220 nm. To balance the ER and IL performances of proposed polarizer, we set w_2 as 220 nm in the following analysis.

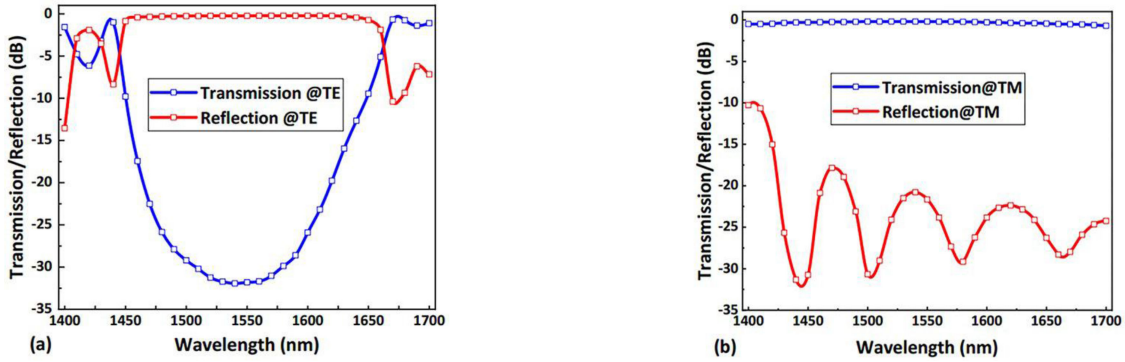

Fig. 6. Wavelength dependence of the proposed device. (a) TE mode input. (b) TM mode input.

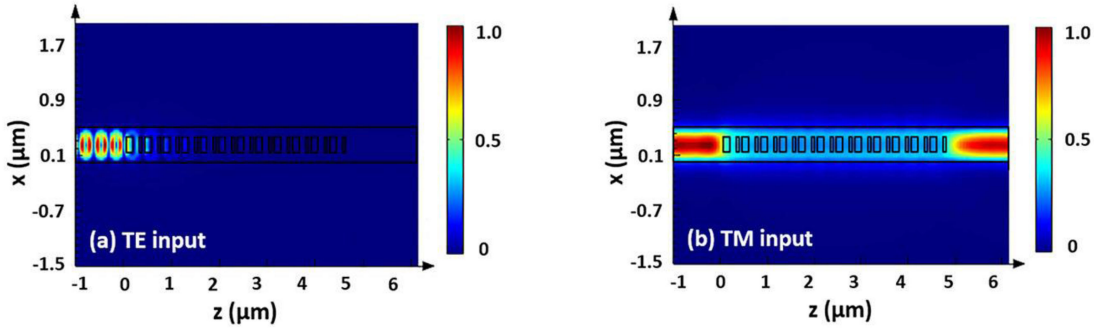

Fig. 7. Light distribution of the proposed polarizer. (a) TE mode input. (b) TM mode input. The dimensions are $w_1 = 500$ nm, $w_2 = 220$ nm, $\Lambda = 400$ nm, $\eta_1 = 0.3$ and $\eta_2 = 0.7$.

The wavelength dependence of the designed polarizer for the TE and TM polarized modes are presented in Fig. 6, where $w_1 = 500$ nm, $w_2 = 220$ nm, $\mathbf{\Lambda_1 = \Lambda_2 = 200}$ nm, $\eta_1 = \mathbf{0.3}$, $\eta_2 = \mathbf{0.7}$ and $N = 13$, respectively. The corresponding length of the device is $L = 5.2$ μm, which is shorter than the previous studies [12], [14], [15]. From these figures, one can see that the transmission response for the TE mode is low than -20.31 dB and the reflection response is higher than -0.375 dB from 1465 nm to 1620 nm, showing a significant Bragg reflection. In contrast, for TM mode, the transmission is higher than -0.646 dB and the reflection is lower than -10.68 dB in the whole calculation region. Considering the reflected light will bring adverse effects on other optical components such as laser sources and optical amplifiers, nonreciprocal optical devices like isolators [37] or polarization-independent circulators [38] should be placed in front of the present polarizer to reduce the negative effects of the reflections. At the operating wavelength of 1550 nm, the ER and IL are 31.63 dB and 0.18 dB, respectively. Since the present device is perfectly symmetric along the propagation direction, theoretically the TM to TE conversion is ignored in this device. For the proposed polarizer, a high ER ($>$20 dB) and low IL ($<$0.32 dB) has been achieved in the wavelength range from 1465 to 1620 nm, extending the bandwidth to 155 nm.

Fig. 7(a)–(b) show the simulated light distribution in the designed polarizer for TE and TM polarizations at the operation wavelength of 1550 nm, respectively. It can be seen that the injected TE mode is reflected by the embedded SWG waveguide with a high efficiency, while the injected TM mode passes through the device with almost no affect. In this way, an ultra-compact TM-pass polarizer with high performance is realized.

The fabrication tolerance caused by the strip waveguide width (w_1) variation is analyzed. The calculated transmission/reflection features of the present polarizer as the function of waveguide width w_1 for both two polarization states are shown in Fig. 8. Here we assume that the SWGs

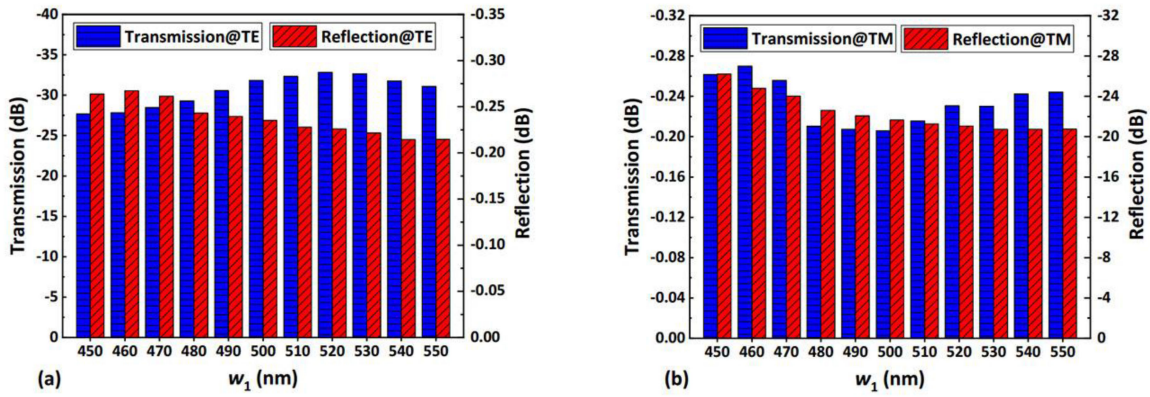

Fig. 8. Transmission and reflection responses of the device as a function of strip waveguides width w_1. (a) TE mode input. (b) TM mode input. The other dimensions are $\Lambda = 400$ nm, $\eta_1 = 0.3$, $\eta_2 = 0.7$ and $N = 13$.

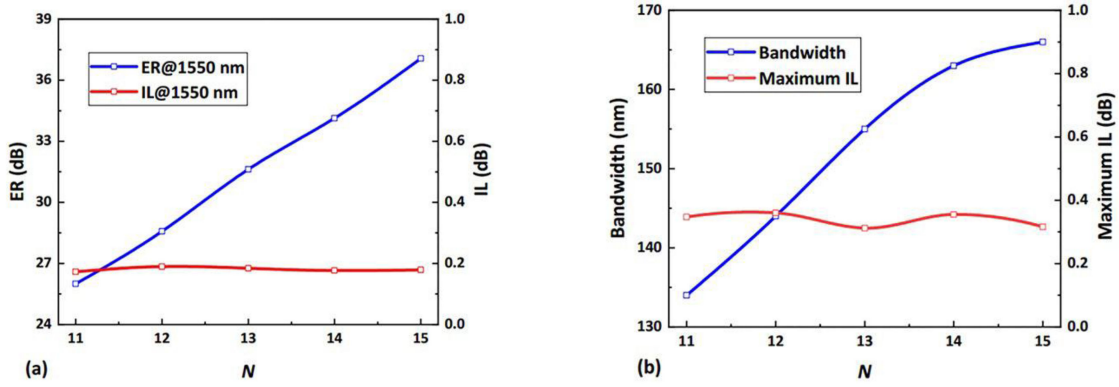

Fig. 9. (a) ER and IL of the device as a function of period number N at operation wavelength of 1550 nm. (b) Bandwidth with ER $>$ 20 dB and maximum IL in the effective working bandwidth as a function of period number N.

waveguides width w_2 has the same variation ratio. From Fig. 8(a) one can see that for TE mode the transmission varies from -32.83 dB to -27.67 dB and the reflection varies from -0.267 dB to -0.214 dB when the waveguide width w_1 changes from 450 nm to 550 nm. For the TM mode, the transmission varies from -0.269 dB to -0.206 dB and the reflection varies from -26.21 dB to -20.72 dB in this waveguide width variation range. In the whole calculation region, the minimum value of ER and the maximum value of IL are 27.13 dB and 0.27 dB, respectively, shows a large fabrication tolerance.

Finally, the relationship between device performance and period number N is also studied. Fig. 9(a) shows the calculated ER and IL of the TM polarization as a function of period number N at the operation wavelength 1550 nm. It can see that the IL is insensitive to N variation while the ER is increased linearly with the increasing of N. This is because the Bragg reflection efficiency of TE mode is enhanced as the period number *N* increases. From Fig. 9(b) one can see that the bandwidth for ER $>$ 20 dB is increased from 135 nm to 167 nm when the period number increases from 11 to 15. Similarly, the maximum values of IL over such bandwidth are fluctuated around 0.34 dB, achieving a low loss transmission. By increasing the period number, a higher performance TM-pass polarizer will be developed.

Table 2 list the comparison between the latest reported TM-pass polarizers and our work, where the main indicators such as highest IL and lowest ER in the effective bandwidth ranges are

TABLE 2
Comparison of Various On-Chip TM-Pass Polarizers

Reference	[11]	[12]	[13]	[14]	[15]	Our work
Length (μm)	1.2	23	2.5	150	15	5.2
IL (dB)	1.5	2.5	0.95	3	3	0.32
ER (dB)	11.5	20	10	40	20	20
Bandwidth (nm)	400	140	130	100	50	155
CMOS compatibility	No	No	No	No	No	Yes

mentioned. Compared with the reported works, our device has the lowest IL, short length and an acceptable bandwidth.

4. Conclusions

In conclusion, we have proposed a novel TM-pass polarizer based on the Bragg reflection in a silicon-based strip waveguide with two SWGs waveguides embedded in the center place. For the present device, the structure dimensions are optimized to make sure that only the Bloch wave of TM polarization is supported in the present device. When the light transmits along the strip waveguide, the inject TM mode passes through the device directly with a low propagation loss, while the inject TE mode is efficiently reflected by the embedded SWG structure. Simulation results show that an ultra-compact TM-pass polarizer with length of 5.2 μm is achieved. The ER and IL of the polarizer are only 31.63 dB and 0.18 dB, respectively, at the operation wavelength of 1550 nm. It has also been shown that in the wavelength range from 1465 nm to 1620 nm, the present polarizer still works well with a decent ER ($>$20 dB) and low IL (IL $<$ 0.32 dB), extending the effective working bandwidth to 155 nm. Furthermore, the bandwidth can be further improved by increasing the period number. Finally, the proposed polarizer can be fabricated with only one etch steep, which will greatly reduce the difficulty level of fabrication. Benefit from these advantages, the suggested TM-pass polarizer will have a potential application in the photonic integrated circuits.

References

[1] C. R. Doerr, "Silicon photonic integration in telecommunications," *Front. Phys.*, vol. 3, pp. 1–16, Aug. 2015, doi: 10.3389/fphy.2015.00037.
[2] D. Dai, J. Bauters, and J. E. Bowers, "Passive technologies for future large-scale photonic integrated circuits on silicon: Polarization handling, light non-reciprocity and loss reduction," *Light Sci. Appl.*, vol. 1, no. 3, pp. e1–e1, Mar. 2012, doi: 10.1038/lsa.2012.1.
[3] H. Xu and Y. Shi, "On-Chip silicon TE-pass polarizer based on asymmetrical directional couplers," *IEEE Photon. Technol. Lett.*, vol. 29, no. 11, pp. 861–864, Jun. 2017.
[4] J. Zhang, E. Cassan, and X. Zhang, "Wideband and compact TE-pass/TM-stop polarizer based on a hybrid plasmonic bragg grating for silicon photonics," *J. Lightw. Technol.*, vol. 32, no. 7, pp. 1383–1386, Apr. 2014, doi: 10.1109/JLT.2014.2302304.
[5] X. Yin *et al.*, "Ultra-Broadband TE-pass polarizer using a cascade of multiple few-layer graphene embedded silicon waveguides," *J. Lightw. Technol.*, vol. 34, no. 13, pp. 3181–3187, Jul. 2016, doi: 10.1109/JLT.2016.2547896.
[6] N. Abadía *et al.*, "CMOS-compatible multi-band plasmonic TE-pass polarizer," *Opt. Express*, vol. 26, no. 23, pp. 30292–30304, Nov. 2018, Art no. 30292, doi: 10.1364/OE.26.030292.
[7] B. Bai, F. Yang, and Z. Zhou, "Demonstration of an on-chip TE-pass polarizer using a silicon hybrid plasmonic grating," *Photon. Res.*, vol. 7, no. 3, pp. 289–293, Mar. 2019, doi: 10.1364/PRJ.7.000289.
[8] A. Densmore *et al.*, "A silicon-on-insulator photonic wire based evanescent field sensor," *IEEE Photon. Technol. Lett.*, vol. 18, no. 23, pp. 2520–2522, Dec. 2006, doi: 10.1109/LPT.2006.887374.
[9] H. Zafar, M. Odeh, A. Khilo, and M. S. Dahlem, "Broadband silicon TM-pass polarizer using a slot-assisted periodic waveguide," in *Proc. IEEE Photon. Conf.*, San Antonio, TX, USA, 2019, pp. 1–2, doi: 10.1109/IPCon.2019.8908454.
[10] Q. Wang and S.-T. Ho, "Ultracompact TM-pass silicon nanophotonic waveguide polarizer and design," *IEEE Photon. J.*, vol. 2, no. 1, pp. 49–56, Feb. 2010.

[11] T. K. Ng, M. Z. M. Khan, A. Al-Jabr, and B. S. Ooi, "Analysis of CMOS compatible Cu-based TM-pass optical polarizer," *IEEE Photon. Technol. Lett.*, vol. 24, no. 9, pp. 724–726, May 2012.

[12] W. Yu, S. Dai, Q. Zhao, J. Li, and J. Liu, "Wideband and compact TM-pass polarizer based on hybrid plasmonic grating in LNOI," *Opt. Express*, vol. 27, no. 24, pp. 34857–34863, Nov. 2019, Art no. 34857, doi: 10.1364/OE.27.034857.

[13] B. Bai, L. Liu, R. Chen, and Z. Zhou, "Low loss, compact TM-pass polarizer based on hybrid plasmonic grating," *IEEE Photon. Technol. Lett.*, vol. 29, no. 7, pp. 607–610, Apr. 2017.

[14] X. Hu and J. Wang, "Ultrabroadband compact graphene–silicon TM-pass polarizer," *IEEE Photon. J.*, vol. 9, no. 2, pp. 1–10, Apr. 2017.

[15] Md. G. Saber, N. Abadía, and D. V. Plant, "CMOS compatible all-silicon TM pass polarizer based on highly doped silicon waveguide," *Opt. Express*, vol. 26, no. 16, pp. 20878–20887, Aug. 2018, Art no. 20878, doi: 10.1364/OE.26.020878.

[16] P. J. Bock *et al.*, "Subwavelength grating periodic structures in silicon-on-insulator: a new type of microphotonic waveguide," *Opt. Express*, vol. 18, no. 19, pp. 20251–20262, Sep. 2010, Art no. 20251, doi: 10.1364/OE.18.020251.

[17] Z. Ruan, L. Shen, S. Zheng, and J. Wang, "Subwavelength grating slot (SWGS) waveguide on silicon platform," *Opt. Express*, vol. 25, no. 15, pp. 18250–18264, Jul. 2017, Art no. 18250. doi: 10.1364/OE.25.018250.

[18] J. Wang, I. Glesk, and L. R. Chen, "Subwavelength grating filtering devices," *Opt. Express*, vol. 22, no. 13, pp. 15335–15345, Jun. 2014, Art no. 15335, doi: 10.1364/OE.22.015335.

[19] V. Donzella, A. Sherwali, J. Flueckiger, S. Talebi Fard, S. M. Grist, and L. Chrostowski, "Sub-wavelength grating components for integrated optics applications on SOI chips," *Opt. Express*, vol. 22, no. 17, pp. 21037–21050, Aug. 2014, Art no. 21037, doi: 10.1364/OE.22.021037.

[20] Y. Wang *et al.*, "Compact broadband directional couplers using subwavelength gratings," *IEEE Photon. J.*, vol. 8, no. 3, pp. 1–8, Jun. 2016.

[21] L. Liu, Q. Deng, and Z. Zhou, "Subwavelength-grating-assisted broadband polarization-independent directional coupler," *Opt. Lett.*, vol. 41, no. 7, pp. 1648–1651, Apr. 2016, doi: 10.1364/OL.41.001648.

[22] B. Naghdi and L. R. Chen, "Silicon photonic contradirectional couplers using subwavelength grating waveguides," *Opt. Express*, vol. 24, no. 20, pp. 23429–23438, Oct. 2016, Art no. 23429, doi: 10.1364/OE.24.023429.

[23] Z. Cheng and H. K. Tsang, "Experimental demonstration of polarization-insensitive air-cladding grating couplers for silicon-on-insulator waveguides," *Opt. Lett.*, vol. 39, no. 7, pp. 2206–2209, Apr. 2014, doi: 10.1364/OL.39.002206.

[24] L. Liu, Q. Deng, and Z. Zhou, "Manipulation of beat length and wavelength dependence of a polarization beam splitter using a subwavelength grating," *Opt. Lett.*, vol. 41, no. 21, pp. 5126–5129, Nov. 2016, doi: 10.1364/OL.41.005126.

[25] T. Huang, Y. Xie, Y. Wu, Z. Cheng, S. Zeng, and P. S. Ping, "Compact polarization beam splitter assisted by subwavelength grating in triple-waveguide directional coupler," *Appl. Opt.*, vol. 58, no. 9, pp. 2264–2268, Mar. 2019, doi: 10.1364/AO.58.002264.

[26] Y. Xiong, J. G. Wangüemert-Pérez, D.-X. Xu, J. H. Schmid, P. Cheben, and W. N. Ye, "Polarization splitter and rotator with subwavelength grating for enhanced fabrication tolerance," *Opt. Lett.*, vol. 39, no. 24, pp. 6931–6934, Dec. 2014, doi: 10.1364/OL.39.006931.

[27] Y. Liu *et al.*, "Subwavelength polarization splitter–rotator with ultra-compact footprint," *Opt. Lett.*, vol. 44, no. 18, pp. 4495–4498, Sep. 2019, doi: 10.1364/OL.44.004495.

[28] Y. Xiong, D.-X. Xu, J. H. Schmid, P. Cheben, and W. N. Ye, "High extinction ratio and broadband silicon TE-pass polarizer using subwavelength grating index engineering," *IEEE Photon. J.*, vol. 7, no. 5, pp. 1–7, Oct. 2015.

[29] X. Guan, P. Chen, S. Chen, P. Xu, Y. Shi, and D. Dai, "Low-loss ultracompact transverse-magnetic-pass polarizer with a silicon subwavelength grating waveguide," *Opt. Lett.*, vol. 39, no. 15, pp. 4514–4517, Aug. 2014, doi: 10.1364/OL.39.004514.

[30] D. W. Kim, M. H. Lee, Y. Kim, and K. H. Kim, "Ultracompact transverse magnetic mode-pass filter based on one-dimensional photonic crystals with subwavelength structures," *Opt. Express*, vol. 24, no. 19, pp. 21560–21565, Sep. 2016, Art no. 21560, doi: 10.1364/OE.24.021560.

[31] B. Liu *et al.*, "Silicon photonic bandpass filter based on apodized subwavelength grating with high suppression ratio and short coupling length," *Opt. Express*, vol. 25, no. 10, pp. 11359–11364, May 2017, Art no. 11359, doi: 10.1364/OE.25.011359.

[32] V. Donzella, A. Sherwali, J. Flueckiger, S. M. Grist, S. T. Fard, and L. Chrostowski, "Design and fabrication of SOI micro-ring resonators based on sub-wavelength grating waveguides," *Opt. Express*, vol. 23, no. 4, pp. 4791–4803, Feb. 2015, doi: 10.1364/OE.23.004791.

[33] Z. Cheng, X. Chen, C. Y. Wong, K. Xu, and H. K. Tsang, "Apodized focusing subwavelength grating couplers for suspended membrane waveguides," *Appl. Phys. Lett.*, vol. 101, no. 10, Sep. 2012, Art no. 101104, doi: 10.1063/1.4750071.

[34] D. Ortega, J. M. Aldariz, J. M. Arnold, and J. S. Aitchison, "Analysis of 'quasi-modes' in periodic segmented waveguides," *J. Lightw. Technol.*, vol. 17, no. 2, pp. 369–375, Feb. 1999, doi: 10.1109/50.744265.

[35] R. Halir *et al.*, "Waveguide sub-wavelength structures: A review of principles and applications: Waveguide sub-wavelength structures," *Laser Photon. Rev.*, vol. 9, no. 1, pp. 25–49, Jan. 2015, doi: 10.1002/lpor.201400083.

[36] D. Oser *et al.*, "Subwavelength engineering and asymmetry: two efficient tools for sub-nanometer-bandwidth silicon Bragg filters," *Opt. Lett.*, vol. 43, no. 14, pp. 3208–3211, Jul. 2018, doi: 10.1364/OL.43.003208.

[37] Y. Zhang *et al.*, "Monolithic integration of broadband optical isolators for polarization-diverse silicon photonics," *Optica*, vol. 6, no. 4, pp. 473–478, Apr. 2019, doi: 10.1364/OPTICA.6.000473.

[38] C. J. Firby, P. Chang, A. S. Helmy, and A. Y. Elezzabi, "Versatile broadband polarization-independent optical circulators for nanophotonic integrated circuits," *J. Opt. Soc. Amer. B*, vol. 35, no. 7, pp. 1504–1513, Jul. 2018, doi: 10.1364/JOSAB.35.001504.